Marine Geology 381 (2016) 181–193

Contents lists available at ScienceDirect

Marine Geology

journal homepage: www.elsevier.com/locate/margo

Flow dynamics and mixing processes in hydraulic jump arrays: Implications for channel-lobe transition zones

R.M. Dorrell [a,*], J. Peakall [a], E.J. Sumner [b], D.R. Parsons [c], S.E. Darby [d], R.B. Wynn [e], E. Özsoy [f,g], D. Tezcan [f]

[a] School of Earth and Environment, University of Leeds, Leeds LS2 9JT, UK
[b] Ocean and Earth Science, University of Southampton, Southampton, UK
[c] Department of Geography, Environment and Earth Sciences, University of Hull, UK
[d] Geography and Environment, University of Southampton, Southampton, UK
[e] National Oceanography Centre, Southampton, UK
[f] Institute of Marine Sciences, Middle East Technical University, Erdemli, Mersin, Turkey
[g] Eurasia Institute of Earth Sciences, İstanbul Technical University, İstanbul, Turkey

ARTICLE INFO

Article history:
Received 21 June 2016
Received in revised form 1 September 2016
Accepted 18 September 2016
Available online 20 September 2016

Keywords:
Gravity currents
Hydraulic jumps
Stratification
Channel-lobe transition zone

ABSTRACT

A detailed field investigation of a saline gravity current in the southwest Black Sea has enabled the first complete analysis of three-dimensional flow structure and dynamics of a series of linked hydraulic jumps in stratified, density-driven, flows. These field observations were collected using an acoustic Doppler current profiler mounted on an autonomous underwater vehicle, and reveal that internal mixing processes in hydraulic jumps, including flow expansion and recirculation, provide a previously unrecognised mechanism for grain-size sorting and segregation in stratified density-driven flows. Field observations suggest a newly identified type of hydraulic jump, that is a stratified low Froude number (<1.5–2) subaqueous hydraulic jump, with an enhanced ability to transport sediment downstream of the jump, in comparison to hydraulic jumps in other subaerial and submarine flows. These novel field data underpin a new process-based conceptual model of channel lobe transition zones (CLTZs) that explains the scattered offset nature of scours within such settings, the temporal variations in infill and erosion between adjacent scours, how bed shear stresses are maintained across the CLTZ, and why the locus of deposition is so far downstream of the scour zone.

1. Introduction

Hydraulic jumps are characterised by a sudden decrease in velocity and an increase in thickness of a flow. In the oceans, hydraulic jumps are thought to occur within gravity-driven flows located on the continental slope (Fildani et al., 2006; Fildani et al., 2013; Kostic et al., 2010; Maier et al., 2011), within submarine canyons and channels (Sumner et al., 2013; Covault et al., 2014; Symons et al., 2016), and in channel-lobe transition zones (Wynn et al., 2002; Kostic and Parker, 2006; Macdonald et al., 2011; Shaw et al., 2013; Hofstra et al., 2015). Hydraulic jumps in these contexts have been linked to a range of processes including: erosion and scour generation, bedform formation, flow mixing, and changes in sediment distribution and stratification (Wynn et al., 2002; Cartigny et al., 2011, 2014; Sumner et al., 2013; Hofstra et al., 2015). The distribution of individual scours in linear trains on the continental slope and within canyons and channels, and in broader zones of erosion at the base-of-slope, has been linked in turn to the presence of multiple hydraulic jumps (Kostic et al., 2010; Macdonald et al., 2011).

Field measurements of hydraulic jumps in natural gravity currents are rare (Sumner et al., 2013). Given the paucity of field measurements, knowledge of subaqueous hydraulic jumps has been dominated by physical and numerical modelling (e.g., Komar, 1971; García and Parker, 1989; García, 1993). Research that follows these modelling approaches has focused on two distinct types of hydraulic jump: those formed by unsteady flows that occur in net depositional settings with chutes-and-pools and cyclic steps, and those that are formed by quasi-steady flows (e.g., Waltham, 2004; Kostic and Parker, 2006; Spinewine et al., 2009; Kostic et al., 2010; Cartigny et al., 2011; Kostic, 2011, 2014; Sumner et al., 2013). Chutes-and-pools and cyclic steps are quasi-permanent features bounded by hydraulic jumps, with chutes-and-pools differentiated by their mild slopes upstream of each hydraulic jump (e.g., Taki and Parker, 2005; Spinewine et al., 2009; Cartigny et al., 2014). Unsteady flows forming cyclic steps and chutes-and-pools are associated with Froude numbers >1.5–2 characterised by breaking waves that form periodic surges, whilst quasi-steady flows have lower

* Corresponding author.
E-mail address: r.m.dorrell@leeds.ac.uk (R.M. Dorrell).

http://dx.doi.org/10.1016/j.margeo.2016.09.009

Froude numbers, typically <1.5–2 (Spinewine et al., 2009; Cartigny et al., 2011, 2014). Cyclic steps and chutes-and-pools have been linked to linear scour trains that are prominent on many continental slopes (e.g., Fildani et al., 2006; Kostic et al., 2010), however the formative processes of distributed scour fields in channel-lobe transition zones remain enigmatic (Macdonald et al., 2011).

To address this knowledge gap we: (i) present the first field measurements of an array of subaqueous hydraulic jumps; (ii) demonstrate that these hydraulic jumps are formed by interaction of a low Froude number, ≤1, flow with seafloor topography; and (iii) assess the flow processes within the hydraulic jumps in terms of mixing, fluid entrainment and their spatial influence downstream. We synthesize these observations to propose a novel conceptual model for low Froude number subaqueous hydraulic jumps over scours, and finally to propose a process-based model of channel-lobe transition zones (CLTZ) that addresses the nature of hydraulic jumps across these scour fields. These novel field data, and the new model of a stratified hydraulic jump derived from it, will inform geohazard risk assessment and hydrocarbon extraction in these complex environments.

2. Geological setting

The Mediterranean Sea and Marmara Sea are more saline (~35 ppt) than the adjacent Black Sea (~18 ppt) (Latif et al., 1991; Parsons et al., 2010), creating a sub-aqueous saline exchange flow (gravity current) through the Bosphorus Strait into the southwest Black Sea, Fig. 1 (Latif et al., 1991; Özsoy et al., 2001; Oğuz, 2005; Flood et al., 2009; Parsons et al., 2010; Sözer, 2013; Sumner et al., 2013, 2014). The Mediterranean Sea has a density of ~1026 kg m^{-3} whereas the Black Sea has a density of ~1014 kg m^{-3} (Hiscott et al., 2013; Sumner et al., 2014), forming a relative density difference of 1.3%. This density difference is similar to the density difference between low concentration turbidity currents and ambient seawater (Pirmez and Imran, 2003; Konsoer et al., 2013; Peakall and Sumner, 2015).

The Black Sea shelf gravity current is confined within a sinuous channel (Fig. 1), achieves velocities of up to 1.5 m/s, is up to 30 m thick, and is sufficiently energetic to transport and rework coarse sand (Özsoy et al., 2001; Sumner et al., 2013). There has been extensive debate on the history of the Holocene reconnection of the Mediterranean and Black Seas, in particular on whether this was associated with a catastrophic flood into the Black Sea (e.g., Ryan et al., 1997, 2003; Thom, 2010), or gradual overtopping of the Black Sea into the Mediterranean via the Marmara Sea (e.g., Hiscott et al., 2002, 2007; Aksu et al., 2016). The most recent connection has been estimated at >8 ka to ~11 ka BP (e.g. Ryan et al., 2003; Hiscott et al., 2007; Thom, 2010; Mertens et al., 2012; Aksu et al., 2016), and activation of the channel on the Black Sea Shelf (Fig. 1), constrained through levee development, has been dated to ~7.5 ka BP suggesting that the channel formed subaqueously rather than via a subaerial catastrophic flood (Flood et al., 2009). The inflow to the Black Sea channel has a quasi-steady discharge, except when very strong onshore winds strengthen the Black Sea outflow, blocking the saline-driven inflow (Latif et al., 1991; Özsoy et al., 2001).

From the Strait of the Bosphorus, the main channel curves northwest following the seafloor slope. Upstream of the curved section, the flow passes over a series of steps and scours on the seafloor (Fig. 2). These seafloor features, and the varying width of the channel, force complex adjustment of the flow resulting in flow acceleration, deceleration and development of hydraulic jumps, as discussed in Sections 4 and 5. After this initial bend, the local channel relief decreases and the flow

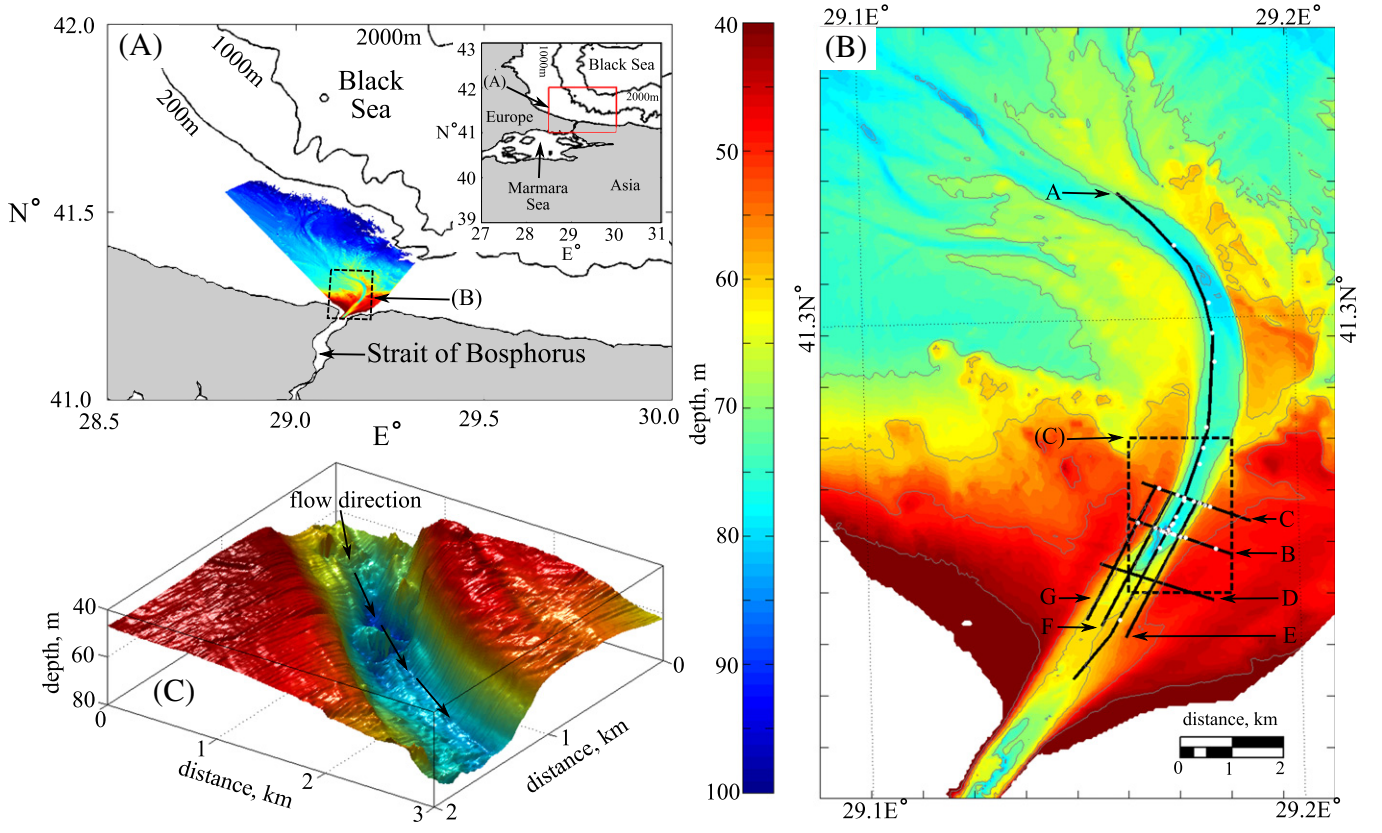

Fig. 1. (a) The location of the field site, in the southwest Black Sea (bathymetry data from GEBCO, 2014). (b) A bathymetric map of the channel system showing depth below sea-level, ADCP Transects A–G, denoted by solid black lines, and locations of CTD profiles, denoted by white circles. (c) Three-dimensional visualization of the channel system, at the location of the largest hydraulic jump located at the intersection of Transects A and B.

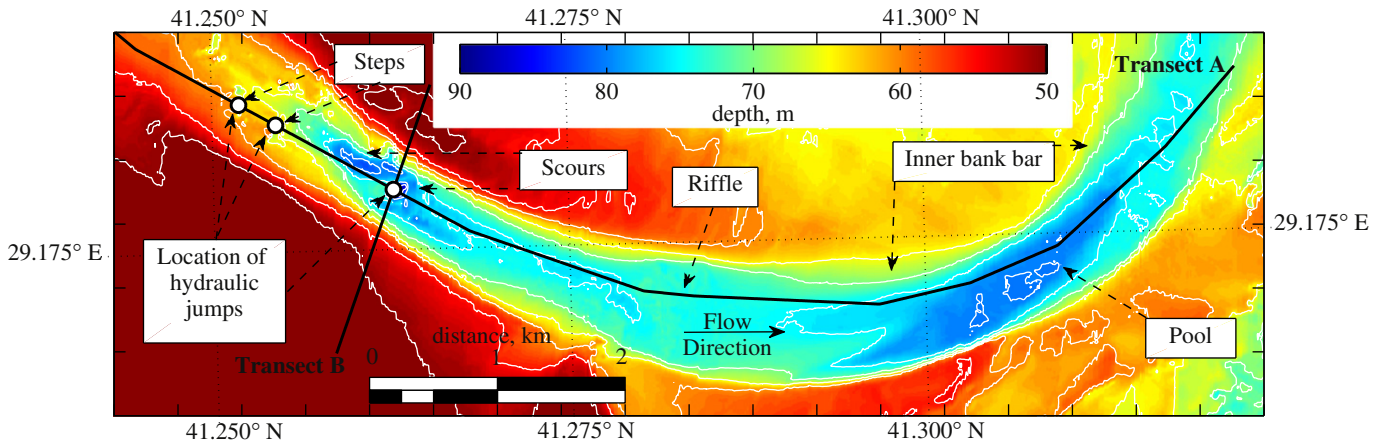

Fig. 2. Detailed bathymetry of the seafloor channel, Fig. 1, with contours at 4 m intervals. Solid black lines denote Transects A and B, which interact at the main channel scour, whilst white circles denote the location of steps (scours) in the bed, and the positions where internal hydraulic jumps were observed at the time of the measurements. Also labelled are the major morphological features of the channel bend.

becomes progressively unconfined. Here the current separates into many smaller flows, forming multi-threaded channels and lobes on the seafloor (Fig. 1b).

3. Data and methods

The velocity of the gravity current was measured in three components using a downward looking 1200 KHz Acoustic Doppler Current Profiler (ADCP), with a vertical bin size of 1 m deployed from the autonomous underwater vehicle (AUV) Autosub3 (see Wynn et al., 2014). Seven transects of flow velocity data were collected, over the steps and scours on the seafloor. Transect A is composed of a single pass, providing an instantaneous time velocity field; Transects B–G are composed from multiple passes, providing time-mean velocity fields. Vertical salinity profiles were measured using a conductivity, temperature, depth (CTD) profiler deployed from a stationary research vessel that had dynamic positioning (R/V Pelagia). The velocity data presented in this study were collected between the 01–02 July 2013; 36 CTD profiles were collected between 02 and 09 July 2013 along the seven velocity transects. CTD profiles taken at the intersect of Transects A and B on the 2nd and 7th of July had a maximum absolute difference of <4%, indicating the flow was relatively steady during this period.

The velocity data were processed using the following steps:

(i) Autosub3's inertial navigation system was corrected for drift using GPS fixes taken at the beginning and end of dives, when the AUV was on the surface.
(ii) The component of velocity resulting from movement of the AUV was removed from the ADCP-derived flow velocity.
(iii) Where large vertical motion was recorded throughout the water column, due to the motion of Autosub3 turning onto a new heading, the ADCP data were discarded.
(iv) Vertical position was corrected, based on the offset of the downwards facing ADCP relative to the AUV's pressure sensor, then converted to depth relative to sea surface.
(v) All data below the maximum ADCP backscatter intensity or within the blanking distance y_b of the seafloor were removed, using $y_b = y_a \sin 2\theta$, where y_a was the altitude of the AUV with respect to the seabed and θ the angle of the profiling beam, 20° (e.g. Sumner et al., 2013).
(vi) Flow velocity within the blanking region y_b of the seafloor was extrapolated assuming a zero slip condition on the seafloor, using Matlab's "PCHIP" interpolation toolkit.
(vii) A single plane of best fit was generated from the repeat data at each transect;
(viii) For each transect velocity vector data were rotated, using the right-hand-rule, and projected onto a single plane derived from the average path of Autosub3 (e.g. Parsons et al., 2010). From this projected cloud of data, a regular grid of flow velocity on each transect was extrapolated using Matlab's linear "griddata" function (determining the time-mean for Transects B–G).

The three components of the processed velocity data are: (i) along plane velocity, which is equivalent to downstream velocity in Transects A and E–G, and inner to outer bank velocity in Transects B–D; (ii) cross plane (normal) velocity, which is equivalent to inner to outer bank velocity in Transects A and E–G, and downstream velocity in Transects B–D; and (iii) vertical velocity. For each transect the flow-ambient fluid interface was defined by the contour of zero downstream flow velocity (Fig. 3a). Here the flow depth, H, is defined as the difference between the flow-ambient-interface and the bed depth, η.

The CTD profiles were processed to provide estimates of the density of the flow along each transect: (i) Density was derived from conductivity, temperature and depth data using the UNESCO (1983) formula; (ii) CTD data were mapped onto associated velocity transects using a linear least squares method to determine the optimal position to minimize distance to sample location; (iii) Depth was converted to relative height above seafloor, to allow comparison with the velocity data; and, (iv) to minimize topographic effects, the CTD data were interpolated between data points using the transformed phase space (x, (y- η)/H), where x is the along channel distance and y the vertical depth with respect to sea level (Sumner et al., 2013). Data interpolation was conducted using Matlab's™ linear "griddata" function, mapping concentration onto the grid describing the single plane of velocity data (Fig. 3b). For Transects D–G insufficient CTD data points meant that flow density profiles could not be generated.

A useful means of characterizing open channel flow behaviour is to compute the Froude number, *Fr*, which is the ratio of the depth-averaged inertial to gravitational forcing. For gravity currents where gravitational forcing depends on the excess density of the flow, this ratio is referred to as the densimetric Froude number, Fr_d (Baines, 1997). For unstratified flows the Froude number is equivalent to the ratio of flow velocity to wave speed and thus a Froude number of unity specifies the transition point from super- to sub-critical flow necessary for a hydraulic jump. The densimetric Froude number may be

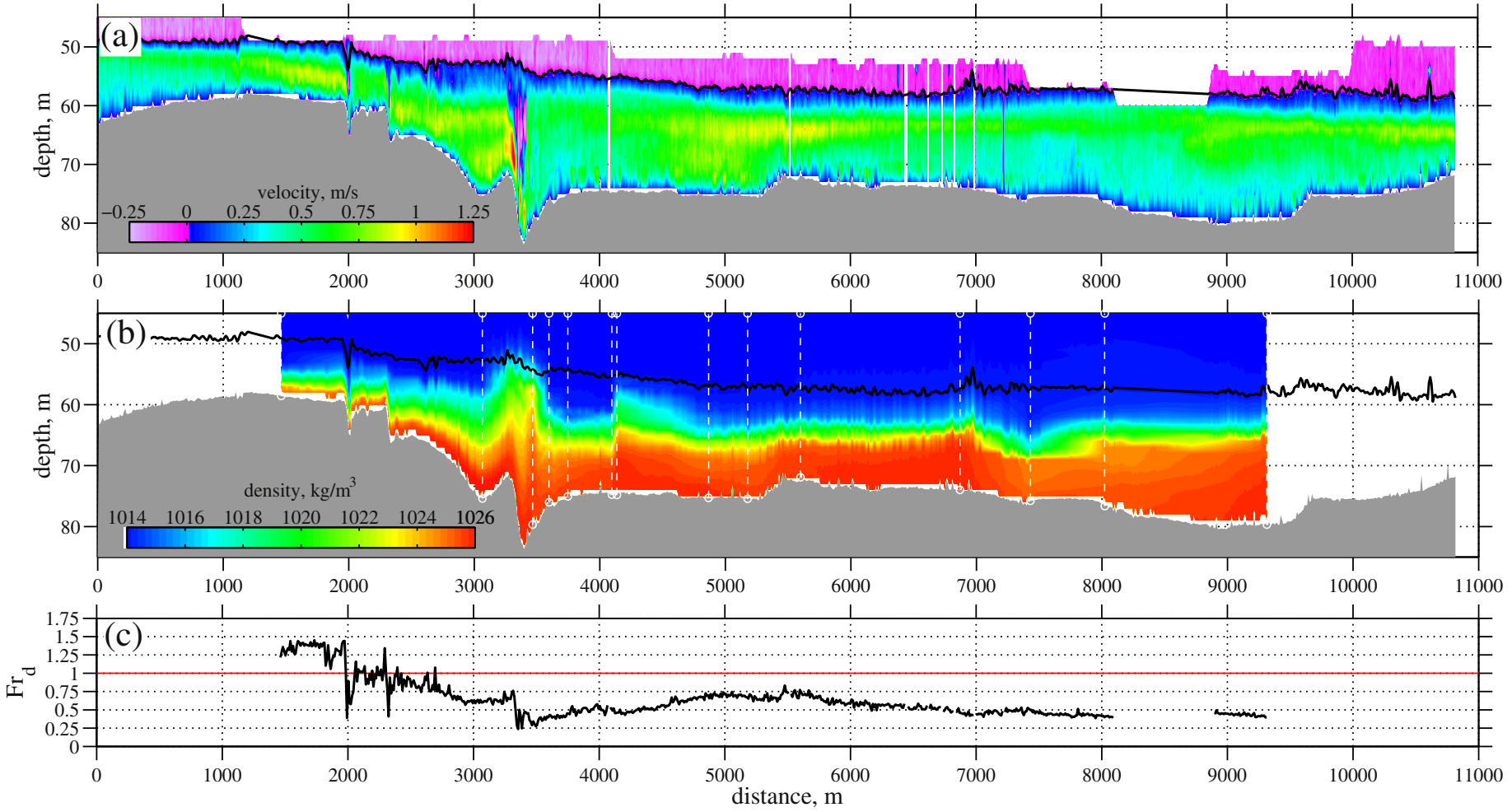
(a)
depth, m
velocity, m/s
−0.25 0 0.25 0.5 0.75 1 1.25
(b)
depth, m
density, kg/m3
1014 1016 1018 1020 1022 1024 1026
(c)
Frd
distance, m

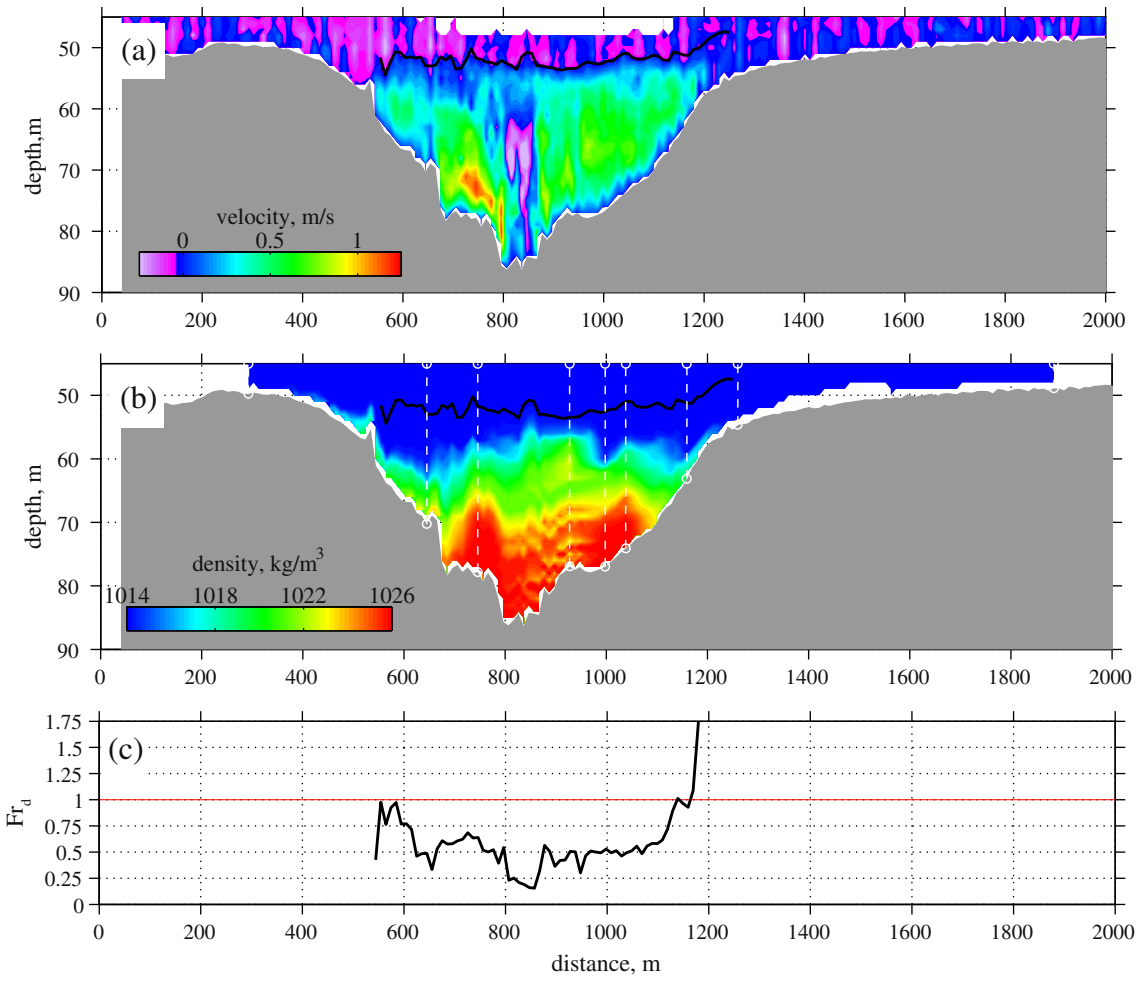

Fig. 4. (a)–(c) Transect B: the downstream velocity (a), density (b) and Froude number (c) cross-sectional profile of the scour at 3400 m in (a). Solid black lines denote the flow velocity - ambient fluid interface, defined by the zero velocity contour, dashed white lines denote locations of CTD profiles and grey shading denotes the seafloor.

derived from flow velocity and density measurements. The depth-averaged Froude number is calculated over the region between the seabed, $y = \eta$, and the flow-ambient fluid interface, $y = \eta + H$. The depth-averaged densimetric Froude number of the density-driven flow is defined as:

$$Fr_d = \frac{\int_\eta^{\eta+H} |u|^2 dy}{\int_\eta^{\eta+H} |u| dy} \frac{1}{\sqrt{g \int_\eta^{\eta+H} \left(\frac{\rho_f}{\rho_a} - 1\right) dy}} \quad (1)$$

Here g denotes specific gravity, $|u|$ velocity magnitude, whilst ρ_f and ρ_a are the current and ambient fluid densities respectively, the latter here being taken as $\rho_a = 1014$ kg/m^3 (Sumner et al., 2013). The first fraction on the right hand side of Eq. (1) describes the velocity averaged over the depth of the flow, according to the method of Ellison and Turner (1959), and the second fraction on the right hand side of Eq. (1) describes the inverse of the gravitational force of the flow arising due to the excess density of the current.

A second useful means of characterizing the behaviour of a stratified, turbulent, current is to define the Richardson gradient number, Ri_g, as the ratio of stratification induced stability of the fluid to shear induced turbulence production

$$Ri_g = \left(-\frac{g}{\rho_f}\frac{\partial \rho_f}{\partial y}\right)\left(\frac{\partial |u|}{\partial y}\right)^{-2}. \quad (2)$$

The first term of the right hand side of Eq. (2) describes the square of the frequency of buoyancy driven fluctuations (Baines, 1997), whilst the second term describes the rate of turbulence production. Theoretically the stability of a steady stratified flow is defined by a value of $Ri_g > 0.25$ (Miles, 1961). However, numerical analysis yields various criteria for stability that range between 0.2 and 1 (Galperin et al., 2007) and it is noted that instability may persist for $Ri_g \gg 1$ in unsteady flows (Majda and Shefter, 1998).

4. Results

Data from the Black Sea field site provide new insight into the dynamics of a stratified gravity driven flow as it passes through a series of hydraulic jumps. The following subsections discuss: the vertical structure of flow in the Black Sea channel and its dynamics, 4.1; the

Fig. 3. (a)–(c) Transect A: the downstream velocity (a), density (b) and Froude number (c) profiles. In (a) and (b) solid black lines denote the flow velocity - ambient fluid interface, defining the zero velocity contour, dashed white lines denote locations of CTD profiles and grey shading denotes the seafloor. In (c) solid black line denotes the densimetric Froude number (Eq. (1)) and the red line denotes the sub-supercritical flow threshold.

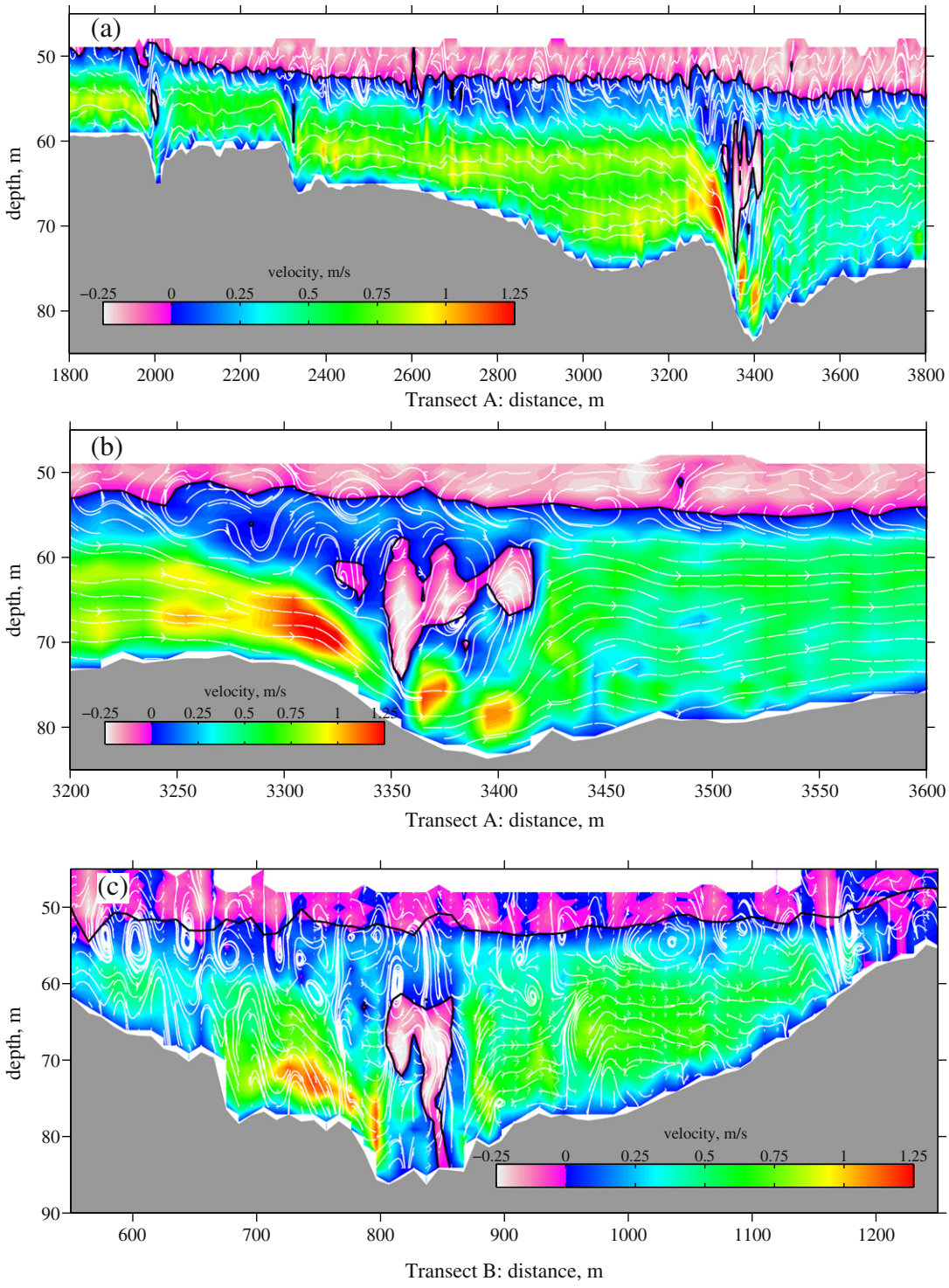

Fig. 5. (a) Downstream flow velocity over the array of scours and hydraulic jumps at the start of Transect A. (b) Detail of downstream flow velocity over the main scour in Transect A. (c) Downstream Flow velocity on the cross-sectional Transect B over the main scour. In (a)–(c) solid colour contour maps describe the downstream velocity and the solid black curves describe the contour of zero flow velocity. White curves denote streamlines of the downstream and vertical flow velocity (a)–(b) and the cross stream (inner to outer bank, Fig. 2) and vertical flow velocity (c). See Figs. 1 and 2 for Transect locations.

effect of internal hydraulic jumps on turbulent mixing within a stratified density-driven flow, 4.2; and the behaviour of bulk flow in and around the Black Sea channel, 4.3.

4.1. Vertical structure of the Black Sea channel density-driven flow

The gravity current formed by the exchange flow through the Strait of Bosphorus has a complex vertical structure as it enters the Black Sea channel system (see Fig. 1 and Sumner et al., 2014). The flow is accelerated by gravity acting on its excess density; and decelerated by frictional drag acting at both the bed, and the interface between the flow and surrounding ambient fluid. This results in the standard velocity profile of a stratified gravity current (Baines, 1997), with flow velocity increasing in magnitude with distance above the seafloor to a maximum near the mid-height of the flow (Fig. 3a). The decreasing cross-sectional shape of the channel (Fig. 2) also acts to accelerate the flow, in accordance

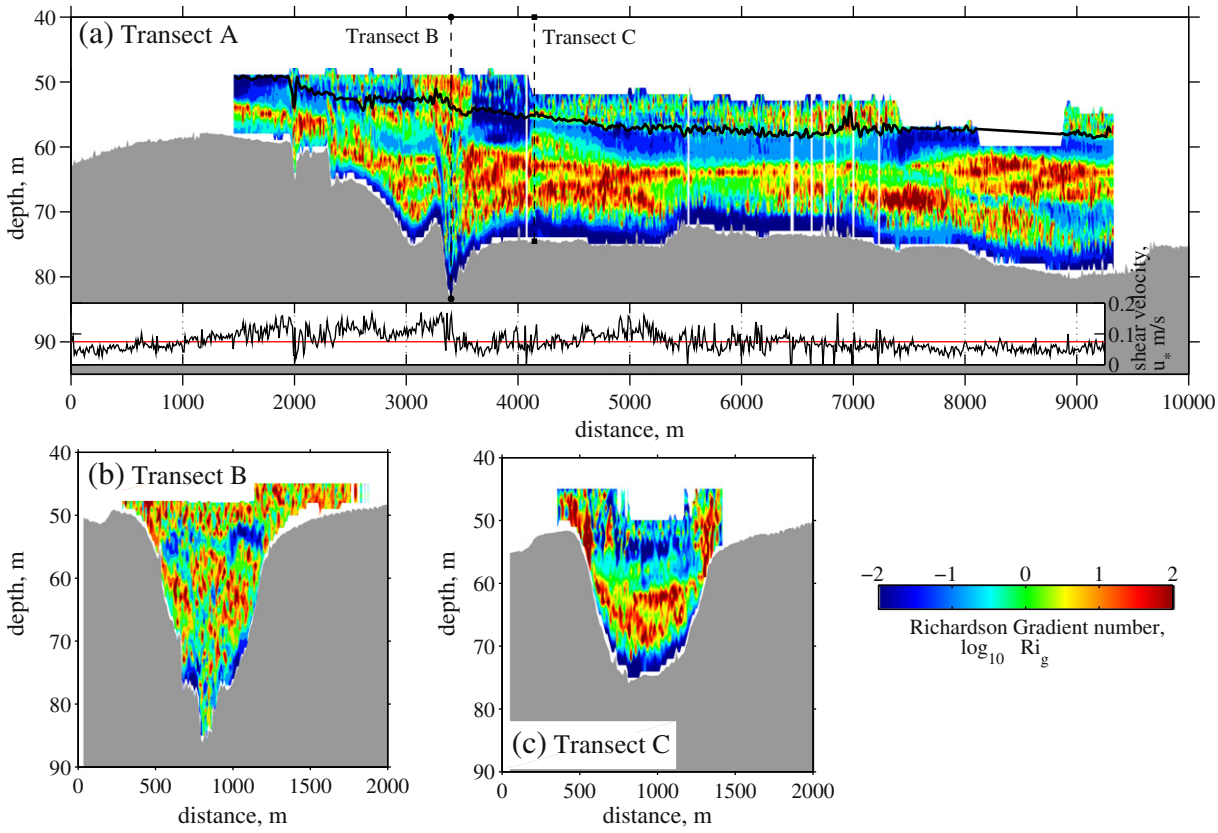

Fig. 6. (a)–(c) Turbulent mixing in Transects A–C respectively, as parameterized by the Richardson gradient number, Ri_g. Inset shows shear velocity, u_*, calculated at 1 m above the bed with mean shear velocity denoted by a solid red line. In (a) dashed black lines denote the location of the cross-sectional Transects B and C. In (a)–(c) solid black curves denote the top of the flow, as defined by the contour of zero downstream flow velocity.

with mass conservation. Moreover, the flow is accelerated and decelerated by changes in the seafloor slope. As indicated in Figs. 3–5, these various forces together result in: flow expansion; vertical flow velocities of >0.3 m/s, two orders of magnitude larger than the mean value; and depth-dependent flow acceleration and deceleration. These features are similar to those seen in super- to subcritical flow transitions in unstratified open-channel flows, with sudden changes in flow velocity and thickness, and it is therefore appropriate to characterise them as internal hydraulic jumps.

The excess density of the flow is vertically stratified due to the entrainment of ambient fluid (Figs. 3–4). The lower half of the flow is approximately uniform with a density ~ 1025 kg/m^3, but above this the flow density drops rapidly to ~1016 kg/m^3 before decreasing more slowly towards a value of ~1014 kg/m^3 near the contour of zero flow velocity used to define the flow's interface with the ambient fluid (Figs. 3b and 4b). Given flow velocity and density profiles the depth-averaged Froude number of the flow may be calculated from Eq. (1), as shown in Figs. 3c and 4c. It is noted that whilst the depth-averaged Froude number changes abruptly across the internal hydraulic jumps shown in Figs. 3c and 4c, it is rarely greater than unity (Sumner et al., 2013).

Examining the hydraulic jumps in more detail shows that small recirculating flow cells are present above the preceding backwards-facing steps, as shown in Fig. 5a and, in greater detail, Fig. 5b–c for the recirculating flow cell above the largest scour. Flow streamlines, denoting the direction that an element of fluid travels in, at a given moment in time, are also shown in Fig. 5. Along Transect A (Fig. 5a–b), the streamlines show that the majority of the flow is closely orientated, parallel to the bed, in the downstream direction. However, over the seafloor scours the streamlines clearly show the recirculation of fluid, composed of fluid moving in the upstream direction, on the back of the internal hydraulic jumps (Fig. 5a–b). From the streamlines it is possible to observe that these recirculation cells are composed of several coherent vortices (Fig. 5b). These recirculation cells are thus similar in composition and formation to the surface rollers generated in open channel hydraulic jumps, as described by Long et al. (1991). At the top of the flow, at the contour of zero flow velocity, used here to define the flow–ambient fluid interface, the streamlines no longer become closely orientated to the bed (Fig. 5a–b). Here, the circular motion captured by the streamlines instead suggests the presence of Kelvin Helmholtz billows at the top of the current. Fig. 5c illustrates that structures with circular motion are also observed transverse to the primary flow.

Figs. 3–5 show that as the flow undergoes an internal hydraulic jump, mixing is enhanced due to the upwards flux of water. This mixing process results in stratification (the vertical variation of excess density) decreasing and flow thickness increasing. Moreover, from Figs. 3–5 it is seen that recirculation cells, described by the presence of upstream-directed flow, are formed as dense near-bed fluid is carried upwards by the expanding flow. Some of this locally denser than ambient fluid sinks under gravity, on the back of the expanding hydraulic jump. However, because relative density gradients are small within the stratified flow, inertia can carry this fluid for a large distance before it sinks. The result is a recirculating cell that extends beyond the upstream initiation of the internal hydraulic jump (Fig. 5b).

4.2. Internal hydraulic jumps and turbulent mixing

The development of the flow as it passes over the steps and scours at the upstream limit of the channel has a significant effect on turbulence and mixing processes within the flow. Here the relative magnitude of turbulence dampening to turbulence production is estimated by calculating the Richardson gradient number Eq. (2) of the flow (Fig. 6).

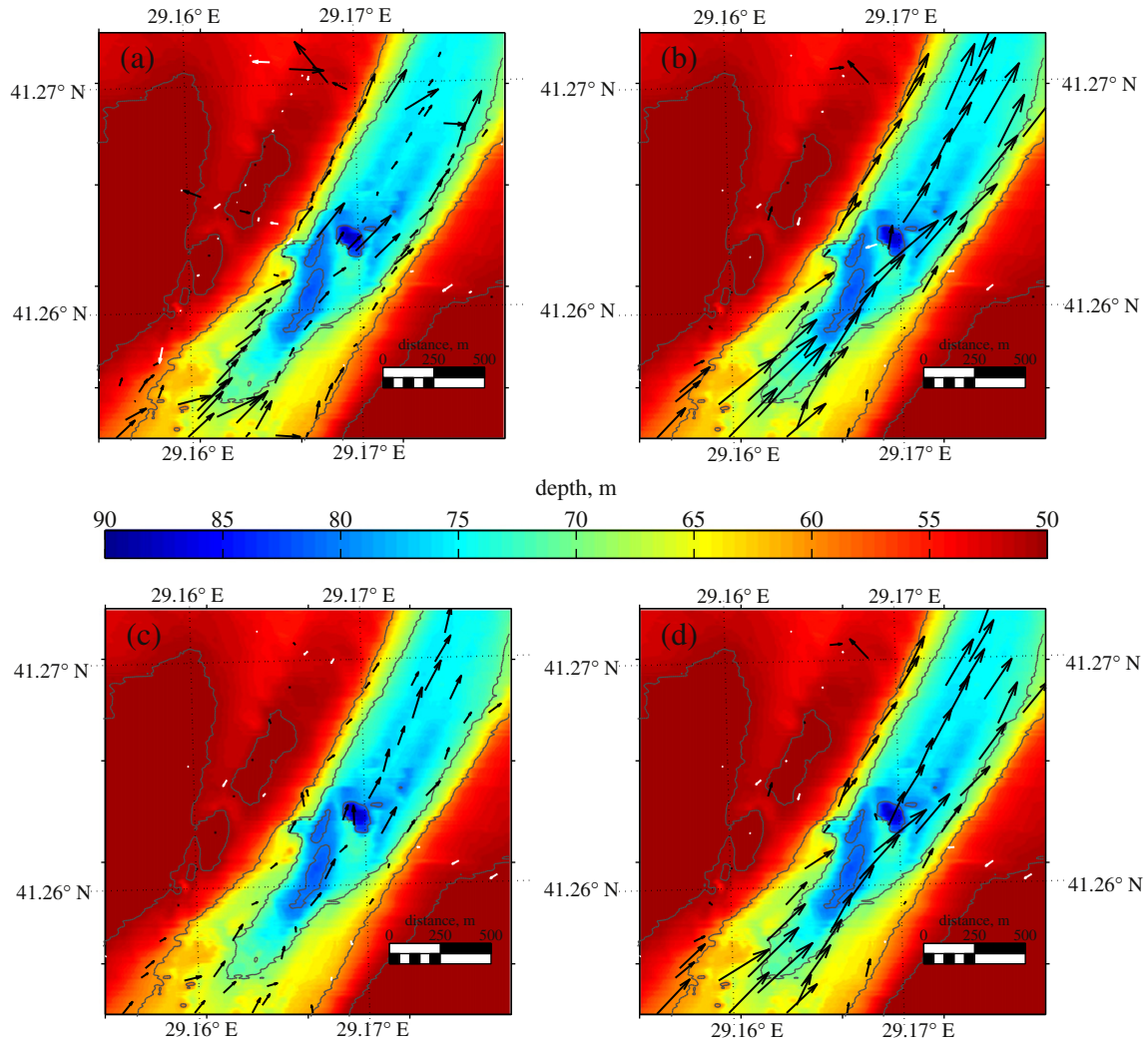

Fig. 7. Depth averaged velocity vector field based on Transects A–G, Fig. 1b, over: (a) bottom 25% of the flow depth H; (b) middle 25–75% of the flow depth H; (c) top 75–100% of the flow depth H; (d) over the entire flow. In (a)–(d): arrows denote the flow velocity vector field with black shading denoting downstream orientated flow and white highlighting upstream orientated flow; the contour plot denotes depth below the surface in metres whilst grey curves depict contours at 8 m intervals.

Fig. 6a shows that along the channel thalweg (Transect A, Fig. 2) the Richardson gradient increases vertically towards the centre of the flow and decreases towards both the lower and upper boundaries of the flow. This is due to the decrease in shear stress at the centre of the flow, near the flow velocity maximum. The large Richardson gradient numbers towards the centre of the flow suggest that shear production is minimized and stratification may act to dampen turbulence, whilst the small Richardson gradient numbers towards the flow-bed and flow-ambient fluid interfaces suggest that shear is generating large amounts of turbulent kinetic energy which may be advected, by fluid motion, into the central region of the flow.

In Fig. 6b and c the Richardson gradient number is also calculated for the cross-sectional Transects B and C. In Transect B (Fig. 6b), the flow is chaotic as the transect sits directly across the scour induced hydraulic jump. Here there is no uniform structure to mixing within the flow, however it is observed that near the flow-ambient fluid interface the Richardson gradient number becomes small as shear production dominates vertical density stratification. Moreover, within 1 km, ~5 scour lengths, downstream of the hydraulic jump at Transect B, the flow has developed a more organized structure (see Transect C; Fig. 6c). Here the turbulent kinetic energy production at the sheared near-bed and flow-ambient fluid interfaces, is clearly separated by a region of low shear, high stratification, that surrounds the velocity maxima of the flow.

4.3. Bulk flow field behaviour over a hydraulic jump in a stratified density driven flow

Transects A–G (Fig. 1b) map the bulk flow behaviour of the internal hydraulic jump associated with the scour located at the intersection of Transects A and B. In Section 4.1 we discussed the bathymetry and depth-resolved flow velocity profiles for this scour and jump (Figs. 3–6). Here we compile the flow velocity profiles from Transects A–G to describe the flow velocity around the scour (Fig. 7). Specifically, Fig. 7a–c show flow behaviour in the basal 25%, the middle 50% and the upper 25% of the flow, respectively. Fig. 7d shows the depth-averaged velocity between the bed and the contour of zero flow velocity, the latter defining the flow-ambient fluid interface. In Fig. 7 the flow at all depths is seen to be predominantly orientated in the direction parallel to the channel sidewalls. Moreover, as frictional stresses diminish, the magnitude of the flow velocity increases away from the bed, away from the flow-ambient fluid interface and away from the channel walls. Whilst the denser than ambient flow is confined in-channel, outer-channel

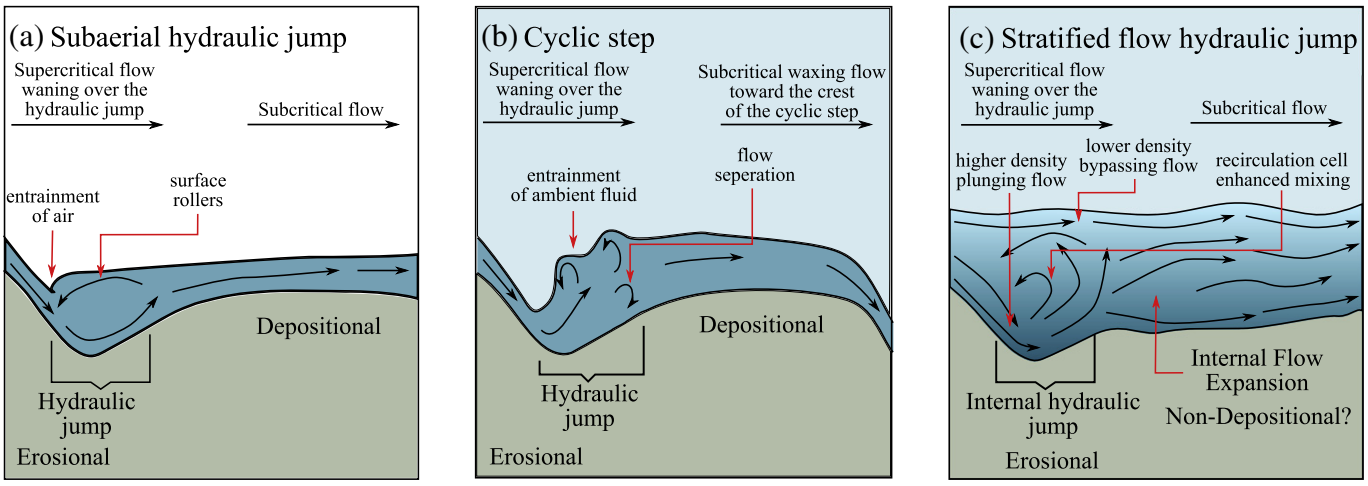

Fig. 8. Sketched behaviour of different types of hydraulic jumps in different environments, including: (a) open channel flow (see, e.g., Rajaratnam, 1967; Long et al., 1991); (b) cyclic steps (see, e.g., Kostic and Parker, 2006; Kostic et al., 2010; Postma et al., 2009; Postma and Cartigny, 2014); (c) stratified subaqueous flow discussed herein.

flow velocities are negligible and predominantly orientated upstream (Fig. 7d).

Lateral deflection of the flow towards the channel banks is observed above the internal hydraulic jump (Fig. 7). Within Transect B (Fig. 4a), the data show that, above the scour, the flow is orientated upstream thus obstructing up to 10% of the downstream flow. However, the deflection is greatest in the central 50% of the flow (Fig. 7b). This is because the recirculation cell associated with the hydraulic jump is elevated above the seafloor, allowing near-bed downstream flow to pass under it, but obstructing downstream flow at greater flow heights. In Fig. 7 the recirculation cell is evident by upstream flow velocities, see also Transect B (Figs. 3–5).

Lateral deflection around the scour diminishes for the top 25% of the flow (Fig. 7c) where flow is predominately bypassed over the scour and internal hydraulic jump (Fig. 5b). Although the recirculation zone sits within the middle reaches of the flow, as highlighted by the negative upstream flow velocities in Fig. 7b, there is no evidence for flow separation in the near-bed region which may influence step height and headwall slope (Allen, 1971). Such near-bed separation is unlikely in the observed stratified hydraulic jump, as if present it must be trapped within the unmeasured near-bed region of the flow, which is limited to 20–30% of the scour height (Section 3).

5. Discussion

5.1. A new model for stratified subaqueous hydraulic jumps

Hydraulic jumps can be classified by the magnitude of the flow height expansion downstream of the jump, a variable that has been shown to be a function of the upstream Froude number in subaerial flows (Baines, 1997). Further, the dynamics of a flow both during and downstream of a hydraulic jump are dependent on the surrounding environment, for example:

1. A single subaerial or submarine hydraulic jump may be formed as flow slows and expands at a break of slope. In the subaerial case (Fig. 8a) surface rollers form a recirculation cell on the top of the flow (Rajaratnam, 1967; Komar, 1971; Long et al., 1991). Depending on water levels after the break in slope, this recirculation cell may extend upstream or downstream of the change in slope.
2. Arrays of linked hydraulic jumps, and co-dependent topography, are found in subaerial and submarine environments. Steep slopes, that generate high depth-averaged Froude number flows, $Fr_d > 1.5 - 2$, provide sufficient motive force to reaccelerate the flow leading to super- to sub- to super-critical flow transition (see Fig. 8b and Kostic et al., 2010). Rapid expansion and reacceleration of the flow enables the flow to adjust within single scour lengths forming linear trains of scours, e.g. cyclic steps (Postma and Cartigny, 2014). Deposition on the lee side of these jumps progressively backfills them, whilst the steps move upstream (Lang and Winsemann, 2013).

In comparison to previous hydraulic jump models the flow dynamics of the observed hydraulic jumps are markedly different. Here the density-driven flow is gravitationally stratified with corresponding higher density, higher velocity flow nearer the bed (except in the near-wall region where flow velocity decreases due to friction). Thus a third type of hydraulic jump is postulated:

3. Rapid deceleration of a pseudo-steady gravity-driven stratified flow results in expanding streamlines, reducing stratification of the high-density lowermost component of the flow. Driven by the expansion of flow streamlines an internal recirculation cell is formed within the flow. As the flow is stratified and the hydraulic jump occurs internally within the flow there exists an uppermost component of the flow that bypasses above it (Figs. 5 and 8c). As the hydraulic jump occurs in the lowermost component of the flow, mixing driven by turbulent expansion, recirculation and deceleration of the flow is contained and entrainment of ambient water is reduced.

Moreover, whilst a hydraulic jump in an unstratified flow requires an upstream Froude number greater than unity (i.e., commonly defined supercritical flow) and downstream Froude number less than unity (i.e., commonly defined subcritical flow), the depth-averaged Froude number observed in the stratified hydraulic jumps was rarely greater than unity (Figs. 3c and 4c). This is because the strict condition necessary for super- subcritical flow transition, and thus a hydraulic jump, is that the flow velocity is greater than the wave speed (Baines, 1997). Whilst the wave speed is equivalent to the denominator of (Eq. (1)) for unstratified open channel flow, this is not true for more complex flows where the wave speed is affected both by topography and flow stratification (see, e.g., Baines, 1997; Thorpe, 2010; Thorpe and Li, 2014). Thus, these observations highlight that the use of depth-averaged parameters to describe stratified density driven flow dynamics is of limited value (Waltham, 2004; Oğuz, 2005; Huang et al., 2009; Sözer, 2013; Sumner et al., 2013).

Stratification has a significant effect on a flow undergoing a hydraulic jump. Thorpe (2010) first reported how, across a hydraulic jump, internal expansion of a monotonically varying stratified flow can theoretically develop into a stratified twin layer flow with two velocity

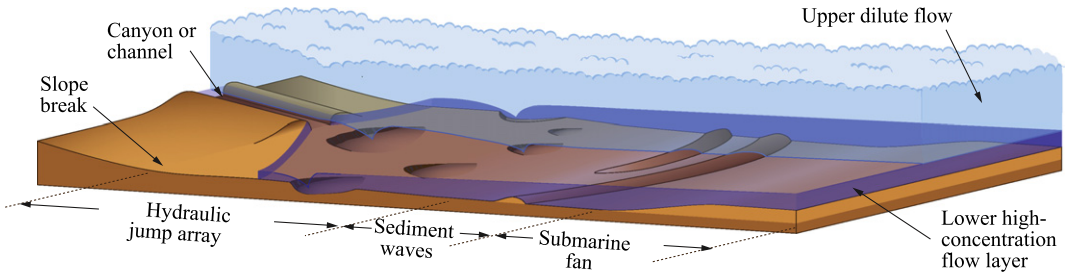

Fig. 9. Schematic channel lobe transition zone showing an array of low Froude number hydraulic jumps occurring at a proportion of scours. The position and proportion of active hydraulic jumps likely varies between flows and as a given flow waxes and wanes. Maintenance of bed shear stress, and local enhancement of suspension downstream of jumps, leads to the primary locus of deposition being beyond the scour field.

maxima. The development of twin layer flow behaviour is observed in expansion of the lowermost component of the flow as it undergoes hydraulic jumps in the Black Sea flow. The twin layer flow exists downstream of the hydraulic jumps, and concomitant backwards facing steps, and persists until destroyed by flow acceleration and recirculation at the scour (Fig. 5a–b). The development of the twin layer flow is also observed in the Richardson gradient number description of turbulence within the flow (Fig. 6a). Here both the twin velocity maxima and the local velocity minima at the mid-height of the flow decrease turbulence production through shear.

5.2. Grainsize sorting and sediment transport across stratified hydraulic jumps

It is inferred from direct observation of the density driven Black Sea flow that flow stratification has an important effect on two fundamental sediment transport processes: grain-size sorting and downstream flow capacity. In sediment-laden flows, transitioning from super to subcritical, the majority of coarse-grained particles, carried near the bed, will pass through the hydraulic jump. Some of the material carried through the jump will be trapped in, and deposited from, the internal recirculation cell. In contrast, some of the finer-grained material, initially more evenly distributed in the water column, will bypass the hydraulic jump, in the upper reaches of the flow, as the flow separates upstream. Thus in the uppermost component of the flow, above the hydraulic jump, the net effect of stratification is to bypass a greater fraction of fine than coarse particulate material. However, within the lowermost component of the flow (containing the hydraulic jump) enhanced mixing and flow expansion will act to distribute sediment more evenly within the flow, thereby decreasing stratification downstream of the jump.

Flow expansion and large vertical flow velocities will rapidly decrease suspended sediment stratification immediately downstream of the hydraulic jump. After this rapid change in sediment stratification, the vertical distribution of suspended particulate material will slowly readjust to local flow conditions (Dorrell and Hogg, 2011). The length scale over which redistributed sediment readjusts determines the spacing of active internal hydraulic jumps. Within the field study site, observed changes in bed slope enabled reacceleration and thus linked hydraulic jumps. However, the length scales between individual jumps are large, ~10 times the scour length (Fig. 6a). This is in contrast to cyclic steps where erosion and deposition appear within a single jump (Postma and Cartigny, 2014). Maintenance of the flow downstream of the hydraulic jump may be explained by the development of the twin velocity maximum, postulated by Thorpe (2010) and observed herein. As the twin velocity maxima are spread vertically over a wide region, the lower velocity maximum remains close to the bed. This enables near-bed shear stresses to be maintained at a similar value across single or multiple hydraulic jumps (Fig. 6a). The ability for flows downstream of a hydraulic jump to maintain near-bed shear stresses means they maintain erosion rates and thus flow capacity (Dorrell et al., 2013a). This mechanism of maintained sediment transport capacity is opposed to current models that suggest that downstream of a hydraulic jump flows are strongly depositional (Pantin and Franklin, 2009; Postma et al., 2009; Symons et al., 2016). Although, with a flow developing a twin velocity maximum, shear and thus turbulent mixing will decrease within the central region of the flow. Ultimately this implies that suspended material will become more concentrated near the seafloor downstream of the jump.

5.3. Implications for channel lobe transition zones (CLTZs)

In contrast to many previous studies which have described the dynamics of depth-averaged Froude number flows, $Fr_d > 1.5 - 2$, found on steep slopes in the proximal reaches of submarine canyon and channel systems (e.g. Fildani et al., 2006, 2013; Lamb et al., 2008; Heinio and Davies, 2009; Normark et al., 2009; Maier et al., 2011), the depth-averaged Froude number flow, $Fr_d \lesssim 1$, described herein provides a suitable analogy with the decelerating flow dynamics of hydraulic jumps that are formed by stratified flow over scours, across lower slopes, in the channel lobe transition zone (CLTZ) (Komar, 1969, 1977; Wynn et al., 2002; Macdonald et al., 2011; Hofstra et al., 2015). CLTZs describe the region of change from confined channels to unconfined lobes, containing widely scattered erosional features and evidence for bypass of sediment (Mutti and Normark, 1987, 1991; Wynn et al., 2002; Hofstra et al., 2015). In particular, new observations presented in this paper provide a possible explanation for some previously enigmatic observations from modern CLTZs. One of these enigmas is the synchronous existence of deposition and erosion within adjacent scours that has recently been observed in CLTZs (Macdonald et al., 2011). Such lateral variations in scour dynamics are not easily interpreted in terms of: i) a single large-scale hydraulic jump at the base of slope affecting the whole CLTZ, or, ii) all scours within a CLTZ exhibiting synchronous hydraulic jumps. The observations instead suggest that in a stratified gravity current, seafloor scours and their concomitant hydraulic jumps affect the flow velocity profile and turbulent mixing processes for multiple scour lengths downstream. Given the persistence of subcritical flow downstream of a hydraulic jump, hydraulic jumps over subsequent scour features may thus be suppressed (Fig. 9). Consequently, for a given input flow, only a proportion of scours in a channel lobe transition zone may exhibit active hydraulic jumps (see Fig. 9 and Sumner et al., 2013). The position and proportion of active hydraulic jumps within a CLTZ may vary between flows as a function of flow magnitude, or as an individual flow waxes and wanes. Moreover, given the negligible change in near-bed stresses downstream of a stratified hydraulic jump, the bulk flow capacity (Dorrell et al., 2013a) of sediment driven gravity currents may remain relatively unchanged. This provides an explanation for the locus of deposition being downstream of broad zones of scour in CLTZs (Wynn et al., 2002; Sumner et al., 2013); vertical turbulent mixing, and maintenance of bed shear stresses enables sediment bypass across these regions. The present work on low Froude number, here $\lesssim 1$, but potentially $< 1.5–2$, hydraulic jump arrays provides a coherent process-

model for the geomorphological observations of channel lobe transition zones.

5.4. The absence of CLTZs in some systems: implications for hydraulic jumps in mud-rich channels

A further enigma is that channel-lobe transition zones are not universal, being associated in modern systems with a high sand/clay ratio, whilst being absent in many mud-rich (high clay/sand ratio) channelised systems such as the Zaire and Mississippi (Mulder and Etienne, 2010; Mulder, 2011). This observed relationship appears to differ to work derived from the ancient where Mutti (1985) defined detached (CLTZ present) and attached (no CLTZ) lobes in larger mud-rich, and smaller sand-rich systems respectively. Many of the observations from modern systems are at a different scale to those in the ancient, and are typically from less tectonically active settings, so there may be multiple parameters controlling CLTZ formation. Here we concentrate on the observations from modern systems. Many large mud-rich channelized systems such as the Zaire (Savoye et al., 2000) and Mississippi (Twichell et al., 1991) show no obvious gap, or scour fields, between channel and lobe. This suggests that the flows are already subcritical by the time they exit the channel, in agreement with modelling that suggests that flows in large submarine channels are subcritical in their distal reaches (Pirmez and Imran, 2003; Dorrell et al., 2013b). Yet, gravity currents in the upper reaches of such systems are thought to be typically supercritical, based on analysis and measurement of flow properties (Pirmez and Imran, 2003; Xu et al., 2004, 2010; Talling et al., 2013), and the presence of linear scour trains (Fildani et al., 2006; Fildani et al., 2013; Heinio and Davies, 2009; Normark et al., 2009). So how do currents undergo the supercritical to subcritical transition and why is there no obvious morphological expression of these hydraulic jumps within these systems?

A number of factors may be responsible for this lack of morphological expression at the super- to sub-critical transition. The present work suggests that the nature of hydraulic jumps in thick, stratified, confined flows may be very different. Mud-rich submarine channels can exhibit strongly stratified flows many tens of metres, to well in excess of a hundred metres, thick (e.g., Peakall et al., 2000; Khripounoff et al., 2003; Savoye et al., 2009; Konsoer et al., 2013; Dorrell et al., 2014; Peakall and Sumner, 2015). Comparison with the Black Sea flows shown herein, suggests that only the lower parts of the flow may undergo a hydraulic jump, with potentially much of the fine-grained upper part of the flow bypassing the jump altogether. Furthermore, large-scale mud-rich submarine channels build towards a graded profile (Kneller, 2003), whilst simultaneously prograding (Normark et al., 1997), thus approaching but never truly reaching grade. These transient graded profiles act to minimize the rate of change of gradient along system, smoothing out areas such as the slope break. Consequently, successive flows may form internal hydraulic jumps at different points within a system, with these migrating downstream and upstream over time as a function of changing dynamics within individual flows (cf. Mulder et al., 2003; Giorgio Serchi et al., 2011; Peakall and Sumner, 2015), rather than being pinned at a specific point such as the slope break. In combination with these longitudinal movements, within an individual flow the thickness of the internal hydraulic jump, and the percentage of the flow involved in the jump, may also alter. Potentially, the net result of this type of internal hydraulic jump in mud-rich submarine channels is to reduce and broaden the zones of erosion and deposition within these systems, leaving no substantive morphological imprint of the super- to sub-critical transition.

6. Conclusions

Here for the first time we examine the three-dimensional flow dynamics of an array of subaqueous hydraulic jumps that are formed by a flow traversing a series of scours, in a natural field example. We demonstrate that these hydraulic jumps have depth-averaged Froude numbers around unity, and that the resulting flow dynamics are very different to higher depth-averaged Froude number (>1.5–2) flows such as those associated with chutes-and-pools and cyclic steps. It is highlighted that in stratified flows depth-averaged Froude numbers do not give an accurate measure of flow criticality. Flows across the scours lead to significant upward velocities, thus aiding sediment suspension and mixing. This enhanced suspension of sediment is maintained downstream of the jump by a flow that exhibits two velocity maxima, that acts to keep high basal shear stresses downstream. The resulting velocity profiles and turbulent mixing profiles are maintained for ~10 scour lengths downstream, in marked contrast to cyclic steps which scale with the scour/bedform length. The persistence of mixing processes and near-bed velocity structure for many scour lengths downstream suggests that the development of hydraulic jumps and concomitant bedform features in close proximity may be suppressed. These observations enable a process-model to be developed for channel lobe transition zones in the deep ocean, suggesting that only a proportion of scours exhibit active hydraulic jumps at any one point in time, and that these may change between flows, and within individual events, as flows wax and wane. The new insights afforded into these processes provide a new explanation of how channel-lobe transition zones typically exhibit an areal distribution of scattered offset scours, rather than the individual linear arrays associated with higher Froude number (>1.5–2) flows associated with cyclic steps. Some mud-rich submarine channel systems do not exhibit channel-lobe transition zones, or an obvious morphological zone associated with the super- to sub-critical transition. The Black Sea results herein suggest that this may in part be due to the development of spatially and temporally varying internal hydraulic jumps in stratified flows, where the hydraulic jump may only affect the lower part of the flow. These results will therefore inform geohazard assessment for placement of seafloor infrastructure (e.g. telecommunications cables and oil/gas pipelines) and hydrocarbon exploration and production (e.g. reservoir connectivity between channel and lobes) in these complex and dynamic environments.

Acknowledgements

This project was funded by Natural Environment Research Council (NERC) grants NE/F020511/1, NE/F020120/1, and NE/F020279/1. We thank the crew of the RV Pelagia for their assistance with cruise planning and operation, and the Marine Autonomous and Robotic Systems (MARS) engineers from NERC National Marine Facilities for AUV operational support. We thank Dave Hodgson for discussions on channel-lobe transition zones. Thierry Mulder and an anonymous reviewer are thanked for their perceptive and constructive comments and feedback.

References

Aksu, A.E., Hiscott, R.N., Yaltirak, C., 2016. Early Holocene age and provenance of a mid-shelf delta lobe south of the strait of Bosphorus, Turkey, and its link to vigorous Black Sea outflow. Mar. Geol. 380, 113–137.
Allen, J.R., 1971. Transverse erosional marks of mud and rock: their physical basis and geological significance. Sediment. Geol. 5, 167–385.
Baines, P.G., 1997. Topographic Effects in Stratified Flows. Cambridge University Press, Cambridge, UK.
Cartigny, M.J., Postma, G., van den Berg, J.H., Mastbergen, D.R., 2011. A comparative study of sediment waves and cyclic steps based on geometries, internal structures and numerical modeling. Mar. Geol. 280 (1), 40–56.
Cartigny, M.J.B., Ventra, D., Postma, G., van den Berg, J.H., 2014. Morphodynamics and sedimentary structures of bedforms under supercritical-flow conditions: new insights from flume experiments. Sedimentology 61, 712–748.
Covault, J.A., Kostic, S., Paull, C.K., Ryan, H.F., Fildani, A., 2014. Submarine channel initiation, filling and maintenance from sea-floor geomorphology and morphodynamic modelling of cyclic steps. Sedimentology 61 (4), 1031–1054.
Dorrell, R.M., Hogg, A.J., 2011. The length and timescales of sediment suspensions to changing flow conditions. J. Hydraul. Eng. 138, 430–439.
Dorrell, R.M., Hogg, A.J., Pritchard, D., 2013a. Polydisperse suspensions: erosion, deposition, and flow capacity. J. Geophys. Res. Earth Surf. 118, 1939–1955.

Dorrell, R.M., Darby, S.E., Peakall, J., Sumner, E.J., Parsons, D.R., Wynn, R.B., 2013b. Superelevation and overspill control secondary flow dynamics in submarine channels. J. Geophys. Res. Oceans 118, 3895–3915.
Dorrell, R.M., Darby, S.E., Peakall, J., Sumner, E.J., Parsons, D.R., Wynn, R.B., 2014. The critical role of stratification in submarine channels: implications for channelization and long runout of flows. J. Geophys. Res. Oceans 119, 2620–2641.
Ellison, T.H., Turner, J.S., 1959. Turbulent entrainment in stratified flows. J. Fluid Mech. 6, 423–448.
Fildani, A., Normark, W.R., Kostic, S., Parker, G., 2006. Channel formation by flow stripping: large-scale scour features along the Monterey East Channel and their relation to sediment waves. Sedimentology 53, 1265–1287.
Fildani, A., Hubbard, S.M., Covault, J.A., Maier, K.L., Romans, B.W., Traer, M., Rowland, J.C., 2013. Erosion at inception of deep-sea channels. Mar. Pet. Geol. 41, 48–61.
Flood, R.D., Hiscott, R.N., Aksu, A.E., 2009. Morphology and evolution of an anastomosed channel network where saline underflow enters the Black Sea. Sedimentology 56, 807–839.
Galperin, B., Sukoriansky, S., Anderson, P.S., 2007. On the critical Richardson number in stably stratified turbulence. Atmos. Sci. Lett. 8, 65–69.
García, M.H., 1993. Hydraulic jumps in sediment-driven bottom currents. J. Hydraul. Eng. 119, 1094–1117.
García, M.H., Parker, G., 1989. Experiments on hydraulic jumps in turbidity currents near a canyon-fan transition. Science 245, 393–396.
General Bathymetric Chart of the Oceans (GEBCO), 2014. GEBCO_14 grid, version 20150318 [Available at] http://www.gebco.netBritish Oceanographic Data Centre, Liverpool, U.K.
Giorgio Serchi, F., Peakall, J., Ingham, D.B., Burns, A.D., 2011. A unifying computational fluid dynamics investigation on the river-like to river-reversed secondary circulation in submarine channel bends. J. Geophys. Res. 116, C06012.
Heinio, P., Davies, R.J., 2009. Trails of depressions and sediment waves along submarine channels on the continental margin of Espirito Santo Basin, Brazil. Geol. Soc. Am. Bull. 121, 698–711.
Hiscott, R.N., Aksu, A.E., Yaşar, D., Kaminski, M.A., Mudie, P.J., Kostylev, V., MacDonald, J., Işler, F.I., Lord, A.R., 2002. Deltas south of the Bosphorus Strait record persistent Black Sea outflow to the Marmara Sea since ~10 ka. Mar. Geol. 190, 95–118.
Hiscott, R.N., Aksu, A.E., Mudie, P.J., Marret, F., Abrajano, T., Kaminski, M., Evans, J., Çakıroğlu II, A., Yaşar, D., 2007. A gradual drowning of the southwestern Black Sea shelf: evidence for a progressive rather than abrupt Holocene reconnection with the eastern Mediterranean Sea through the Marmara Sea gateway. Quat. Int. 167, 19–34.
Hiscott, R.N., Aksu, A.E., Flood, R.D., Kostylev, V., Yaşar, D., 2013. Widespread overspill from a saline density-current channel and its interaction with topography on the south-west Black Sea shelf. Sedimentology 60, 1639–1667.
Hofstra, M., Hodgson, D.M., Peakall, J., Flint, S.S., 2015. Giant scour-fills in ancient channel-lobe transition zones: formative processes and depositional architecture. Sediment. Geol. 329, 98–114.
Huang, H., Imran, J., Pirmez, C., Zhang, Q., Chen, G., 2009. The critical densimetric Froude number of subaqueous gravity currents can be non-unity or non-existent. J. Sediment. Res. 79, 479–485.
Khripounoff, A., Vangriesheim, A., Babonneau, N., Crassous, P., Dennielou, B., Savoye, B., 2003. Direct observation of intense turbidity current activity in the Zaire submarine valley at 4000 m water depth. Mar. Geol. 194, 151–158.
Kneller, B., 2003. The influence of flow parameters on turbidite slope channel architecture. Mar. Pet. Geol. 20, 901–910.
Komar, P.D., 1969. The channelized flow of turbidity currents with application to Monterey deep sea fan channel. J. Geophys. Res. B 74, 4544–4558.
Komar, P.D., 1971. Hydraulic jumps in turbidity currents. Geol. Soc. Am. Bull. 82, 1477–1488.
Komar, P.D., 1977. Computer simulation of turbidity current flow and the study of deep-sea channels and fan sedimentation. In: Goldberg, E.D., McCave, I.N., O'Brien, J.J., Steele, J.H. (Eds.), The Sea: Ideas and Observations on Progress in the Study of the Seas, Volume 6, Marine Modelling. John Wiley, New York, pp. 603–621.
Konsoer, K., Zinger, J., Parker, G., 2013. Bankfull hydraulic geometry of submarine channels created by turbidity currents: relations between bankfull channel characteristics and formative flow discharge. J. Geophys. Res. Earth Surf. 118, 216–228.
Kostic, S., 2011. Modeling of submarine cyclic steps: controls on their formation, migration, and architecture. Geosphere 7, 294–304.
Kostic, S., 2014. Upper flow regime bedforms on levees and continental slopes: turbidity current flow dynamics in response to fine-grained sediment waves. Geosphere 10, 1094–1103.
Kostic, S., Parker, G., 2006. The response of turbidity currents to a canyon–fan transition: internal hydraulic jumps and depositional signatures. J. Hydraul. Res. 44, 631–653.
Kostic, S., Sequeiros, O., Spinewine, B., Parker, G., 2010. Cyclic steps: a phenomenon of supercritical shallow flow from the high mountains to the bottom of the ocean. J. Hydro Environ. Res. 3, 167–172.
Lamb, M.P., Parsons, J.D., Mullenbach, B.L., Finlayson, D.P., Orange, D.L., Nittrouer, C.A., 2008. Evidence for superelevation, channel incision, and formation of cyclic steps by turbidity currents in Eel Canyon, California. Geol. Soc. Am. Bull. 120, 463–475.
Lang, J., Winsemann, J., 2013. Lateral and vertical facies relationships of bedforms deposited by aggrading supercritical flows: from cyclic steps to humpback dunes. Sediment. Geol. 296, 36–54.
Latif, M.A., Özsoy, E., Oğuz, T., Ünlüata, Ü., 1991. Observations of the Mediterranean inflow into the Black Sea. Deep Sea Res. Part A 38, S711–S723.
Long, D., Rajaratnam, N., Steffler, P.M., Smy, P.R., 1991. Structure of flow in hydraulic jumps. J. Hydraul. Res. 29 (2), 207–218.
Macdonald, H.A., Wynn, R.B., Huvenne, V.A., Peakall, J., Masson, D.G., Weaver, P.P., McPhail, S.D., 2011. New insights into the morphology, fill, and remarkable longevity (>0.2 my) of modern deep-water erosional scours along the northeast Atlantic margin. Geosphere 7, 845–867.
Maier, K.L., Fildani, A., Paull, C.K., Graham, S.A., McHargue, T.R., Caress, D.W., McGann, M., 2011. The elusive character of discontinuous deep-water channels: new insights from Lucia Chica channel system, offshore California. Geology 39, 327–330.
Majda, A.J., Shefter, M.G., 1998. Elementary stratified flows with instability at large Richardson number. J. Fluid Mech. 376, 319–350.
Mertens, K.N., Bradley, L.R., Takano, Y., Mudie, P.J., Marret, F., Aksu, A.E., Hiscott, R.N., Verleye, T.J., Mousing, E.A., Smyrnova, L.L., Bagheri, S., Mansor, M., Pospelova, V., Matsuoka, K., 2012. Quantitative estimation of Holocene surface salinity variation in the Black Sea using dinoflagellate cyst process length. Quat. Sci. Rev. 39, 45–59.
Miles, J.W., 1961. On the stability of heterogeneous shear flows. J. Fluid Mech. 10, 496–508.
Mulder, T., 2011. Gravity processes and deposits on continental slope, rise and abyssal plains. In: Hüneke, H., Mulder, T. (Eds.), Deep-sea Sediments. Developments in Sedimentology Vol. 63, pp. 25–148.
Mulder, T., Etienne, S., 2010. Lobes in deep-sea turbidite systems: state of the art. Sediment. Geol. 229, 75–80.
Mulder, T., Syvitski, J.P.M., Migeon, S., Faugeres, J.C., Savoye, B., 2003. Marine hyperpycnal flows: initiation, behaviour and related deposits. A review. Mar. Pet. Geol. 20, 861–882.
Mutti, E., 1985. Turbidite systems and their relations to depositional sequences. In: Zuffa, G.G. (Ed.), Provenance of Arenites. Reidel Publishing Company, Dordrecht, pp. 65–93.
Mutti, E., Normark, W.R., 1987. Comparing examples of modern and ancient turbidite systems: problems and concepts. In: Leggett, J.K., Zuffa, G.G. (Eds.), Marine Clastic Sedimentology: Concepts and Case Studies. Graham and Trotman, London, pp. 1–38.
Mutti, E., Normark, W.R., 1991. An integrated approach to the study of turbidite systems. In: Weimer, P., Link, M.H. (Eds.), Seismic Facies and Sedimentary Processes of Submarine Fans and Turbidite Systems. Springer, New York, pp. 75–106.
Normark, W.R., Damuth, J.E., the Leg 155 Sedimentology Group, 1997. Sedimentary facies and associated depositional elements of the Amazon Fan. In: Flood, R.D., Piper, D.J.W., Klaus, A., Peterson, L.C. (Eds.), Proceedings of the Ocean Drilling Programme, Scientific Results, Leg 155. Ocean Drilling Programme, College Station, TX, pp. 611–651.
Normark, W.R., Paull, C.K., Caress, D.W., Ussler III, W., Sliter, R., 2009. Fine-scale relief related to Late Holocene channel shifting within the floor of the upper Redondo Fan, offshore Southern California. Sedimentology 56, 1670–1689.
Oğuz, T., 2005. Hydraulic adjustments of the Bosphorus exchange flow. Geophys. Res. Lett. 32, L06604.
Özsoy, E., Di Iorio, D., Gregg, M.C., Backhaus, J.O., 2001. Mixing in the Bosphorus Strait and the Black Sea continental shelf: observations and a model of the dense water outflow. J. Mar. Syst. 31, 99–135.
Pantin, H.M., Franklin, M.C., 2009. Predicting autosuspension in steady turbidity flow: ignition points and their relation to Richardson numbers. J. Sediment. Res. 79, 862–871.
Parsons, D.R., Peakall, J., Aksu, A.E., Flood, R.D., Hiscott, R.N., Beşiktepe, Ş., Mouland, D., 2010. Gravity-driven flow in a submarine channel bend: direct field evidence of helical flow reversal. Geology 38, 1063–1066.
Peakall, J., Sumner, E.J., 2015. Submarine channel flow processes and deposits: a process-product perspective. Geomorphology 244, 95–120.
Peakall, J., McCaffrey, W.D., Kneller, B.C., 2000. A process model for the evolution, morphology, and architecture of sinuous submarine channels. J. Sediment. Res. 70, 434–448.
Pirmez, C., Imran, J., 2003. Reconstruction of turbidity currents in Amazon Channel. Mar. Pet. Geol. 20, 823–849.
Postma, G., Cartigny, M.J., 2014. Supercritical and subcritical turbidity currents and their deposits - a synthesis. Geology 42, 987–990.
Postma, G., Cartigny, M., Kleverlaan, K., 2009. Structureless, coarse-tail graded Bouma Ta formed by internal hydraulic jump of the turbidity current? Sediment. Geol. 219 (1), 1–6.
Rajaratnam, N., 1967. Hydraulic jumps. Adv. Hydrosci. 4, 197–280.
Ryan, W.B.F., Pitman III, W.C., Major, C.O., Shimkus, K., Maskalenko, V., Jones, G.A., Dimitrov, P., Görür, N., Sakinç, M., Yüce, H., 1997. An abrupt drowning of the Black Sea shelf. Mar. Geol. 138, 119–126.
Ryan, W.B.F., Major, C.O., Lericolais, G., Goldstein, S.L., 2003. Catastrophic flooding of the Black Sea. Annu. Rev. Earth Planet. Sci. 31, 525–554.
Savoye, B., Cochonat, P., Apprioual, R., Bain, O., Baltzer, A., Bellec, V., Beuzart, P., Bourillet, J.-F., Cagna, R., Cremer, M., Crusson, A., Dennielou, B., Diebler, D., Droz, L., Ennes, J.-C., Floch, G., Guiomar, M., Harmegnies, F., Kerbrat, R., Klein, B., Kuhn, H., Landuré, J.-Y., Lasnier, C., Le Drezen, E., Le Formal, J.-P., Lopez, M., Loubrieu, B., Marsset, T., Migeon, S., Normand, A., Nouzé, H., Ondréas, H., Pelleau, P., Saget, P., Séranne, M., Sibuet, J.-C., Tofani, R., Voisset, M., 2000. Structure and recent evolution of the Zaire deepsea fan: preliminary results of the Zaïango 1 and 2 cruises (Angola-Congo margin). Comptes Rendus de l'Academie des Sciences, Serie II. Sciences de la Terre et des Planetes 331, 211–220.
Savoye, B., Babonneau, N., Dennielou, B., Bez, M., 2009. Geological overview of the Angola–Congo margin, the Congo deep-sea fan and its submarine valleys. Deep-Sea Res. II 56, 2169–2182.
Shaw, J., Puig, P., Han, G., 2013. Megaflutes in a continental shelf setting, Placentia Bay, Newfoundland. Geomorphology 189, 12–25.
Sözer, A., 2013. Numerical Modeling of the Bosphorus Exchange Flow Dynamics, Ph.D. Thesis. Institute of Marine Sciences, Middle East Technical University, Erdemli, Mersin, Turkey.

Spinewine, B., Sequeiros, O.E., Garcia, M.H., Beaubouef, R.T., Sun, T., Savoye, B., Parker, G., 2009. Experiments on wedge-shaped deep sea sedimentary deposits in minibasins and/or on channel levees emplaced by turbidity currents. Part II. Morphodynamic evolution of the wedge and the associated bedforms. J. Sediment. Res. 79, 608–628.
Sumner, E.J., Peakall, J., Parsons, D.R., Wynn, R.B., Darby, S.E., Dorrell, R.M., Webb, A., White, D., 2013. First direct measurements of hydraulic jumps in an active submarine density current. Geophys. Res. Lett. 40, 5904–5908.
Sumner, E.J., Peakall, J., Dorrell, R.M., Parsons, D.R., Darby, S.E., Wynn, R.B., Webb, A., White, D., 2014. Driven around the bend: spatial evolution and controls on the orientation of helical bend flow in a natural submarine gravity current. J. Geophys. Res. Oceans 119, 898–913.
Symons, W.O., Sumner, E.J., Talling, P.J., Cartigny, M.J., Clare, M.A., 2016. Large-scale sediment waves and scours on the modern seafloor and their implications for the prevalence of supercritical flows. Mar. Geol. 371, 130–148.
Taki, K., Parker, G., 2005. Transportational cyclic steps created by flow over an erodible bed. Part 1. Experiments. J. Hydraul. Res. 43, 488–501.
Talling, P.J., Paull, C.K., Piper, D.J.W., 2013. How are subaqueous sediment density flows triggered, what is their internal structure and how does it evolve? Direct observations from monitoring of active flows. Earth Sci. Rev. 125, 244–287.
Thom, N., 2010. A hydrological model of the Black and Caspian seas in the late Pleistocene and early–middle Holocene. Quat. Sci. Rev. 29, 2989–2995.
Thorpe, S.A., 2010. Turbulent hydraulic jumps in a stratified shear flow. J. Fluid Mech. 654, 305–350.
Thorpe, S.A., Li, L., 2014. Turbulent hydraulic jumps in a stratified shear flow. Part 2. J. Fluid Mech. 758, 94–120.
Twichell, D.C., Kenyon, N.H., Parson, L., McGregor, B.A., 1991. Depositional patterns of the Mississippi Fan surface: evidence from GLORIA II and high-resolution seismic profiles. In: Weimer, P., Link, M.H. (Eds.), Seismic Facies and Sedimentary Processes of Submarine Fans and Turbidite Systems. Springer, New York, pp. 349–363.
UNESCO, 1983. Algorithms for computation of fundamental properties of seawater. UNESCO Technical Papers in Marine Science 44. UNESCO Division Marine Science, Paris, p. 53.
Waltham, D., 2004. Flow transformations in particulate gravity currents. J. Sediment. Res. 74, 129–134.
Wynn, R.B., Kenyon, N.H., Masson, D.G., Stow, D.A., Weaver, P.P., 2002. Characterization and recognition of deep-water channel-lobe transition zones. AAPG Bull. 86, 1441–1462.
Wynn, R.B., Huvenne, V.A.I., Le Bas, T.P., Murton, B.J., Connelly, D.P., Bett, B.J., Ruhl, H.A., Morris, K.J., Peakall, J., Parsons, D.R., Sumner, E.J., Darby, S.E., Dorrell, R.M., Hunt, J.E., 2014. Autonomous underwater vehicles (AUVs): their past, present and future contributions to the advancement of marine geoscience. Mar. Geol. 352, 451–468.
Xu, J.P., Noble, M.A., Rosenfeld, L.K., 2004. In-situ measurements of velocity structure within turbidity currents. Geophys. Res. Lett. 31, L09311.
Xu, J.P., Swatzenski, P.W., Noble, M., Li, A.-C., 2010. Event-driven sediment flux in Hueneme and Mugu submarine canyons, Southern California. Mar. Geol. 269, 74–88.